Vietnam Journal of Catalysis and Adsorption
Tạp chí xúc tác và hấp phụ Việt Nam

https://chemeng.hust.edu.vn/jca/

Green and facile synthesis of Fe_3O_4 nanoparticles using the *Citrus aurantifolia* fruit juice associated with $NaBH_4$ and its adsorption of Cr(VI) in aqueous solution

Luong Huynh Vu Thanh[1], Dao Lam Gia Hao[1], Phan Thi Diem Trang[1], Pham Minh Tien[1], Tran Thi Bich Quyen[1], Dang Huynh Giao[1], Tran Nguyen Phuong Lan[2,*]

[1] *Department of Chemical Engineering, Can Tho University, Can Tho, VIETNAM.*
[2]*Department of Mechanical Engineering, Can Tho University, Can Tho, VIETNAM*
**Email: tnplan@ctu.edu.vn*

ARTICLE INFO

Received: 15/7/2021
Accepted: 18/8/2021
Published: 20/8/2021

Keywords:

Citrus aurantifolia extract, Adsorption of Cr(VI), Facile synthesis, Green method, Magnetite nanoparticles

ABSTRACT

This work presents a facile and green method using *Citrus aurantifolia* fruit extract for the biosynthesis of magnetite nanoparticles (MNs). The effects of some effective parameters such as temperature, reaction time and the ratio of *Citrus aurantifolia* extract to sodium borohydride on the synthesis were investigated. The synthesized Fe_3O_4 nanoparticles were characterized by X-ray diffraction (XRD), Fourier-transform infrared spectroscopy (FTIR), field emission scanning electron microscopy (FE-SEM), energy-dispersive X- ray spectroscopy (EDX), transmission scanning electron microscopy (TEM), and vibrating sample magnetometer (VSM). The results showed that the MNs were well-monodisperse with the mean size of 50 nm and superparamagnetism value of 40.1 emu/g. Adsorption of Cr(VI) in aqueous solution at pH 2.5 using MNs reached 94.9% for removal of Cr(VI). The main contribution of this work was the synthesis of MNs in an economical and environmental friendly way, achieving size-controlled MNs at mild conditions. A possible mechanism of MNs synthesis was also presented.

Introduction

Hexavalent chromium (Cr(VI)) is one of the most toxic cations which can cause damage to public health and the environment [1]. There are various methods for the treatment of heavy metals in contaminated water, including chemical precipitation, membrane filtration, ion exchange, electrodialysis and photocatalytic degradation [2-4]. Although these methods possess high efficiency but they are costly; thus are restricted in practical applications. Differently, adsorption method is widely used because it is simple and easy to scale up in industrial application. There are plenty of adsorbents that have been applied to remove heavy metal ions, such as zeolite, activated carbon, agricultural by-products. Among these adsorbents, magnetite nanoparticles (MNs) have high potential in the removal of toxic contaminants, such as As(V) [5], methylene blue [6], and Hg(II) [7, 8].

Magnetite nanoparticles (MNs) are widely used in hazardous waste treatment due to its magnetic property, high surface area, chemical stability and low toxicity [9]. For example, Fe_3O_4 nanoparticles were synthesized and functionalized with several functional groups to remediate aqueous solution contaminated by heavy metals [5, 10, 11]. Many reports on MNs synthesis methods are available [12]. However, several limitations and drawbacks were indicated in these

https://doi.org/10.51316/jca.2021.074

methods which usually required special equipment, expensive chemicals and extreme conditions such as inert gas environment, vacuum atmosphere, long reaction time and high reaction temperature. For instance, toxic, corrosive, and flammable chemical substances such as sodium borohydride ($NaBH_4$) was used as a reducing agent to form zero-valence iron nanoparticles before Fe_3O_4 nanoparticles were formed by oxidation [16]. Fe_3O_4 nanoparticles were synthesized at high temperature (120 °C) with long reaction time (2 h) before being annealed at 400 °C for 4 h [14]. Furthermore, in conventional methods the synthesized magnetite nanoparticles were oxidized easily due to the presence of oxidizing agents in solvent (e.g., dissolved oxygen or water); hence stability of these nanoparticles was reduced significantly. To solve this issue, MNs were normally functionalized on their surfaces by using graphene or SiO_2 [15, 16]. Consequently, new synthesis processes using natural extracts have been developed in recent years. These green synthesis methods are not only less harmful to the environment but also are low-cost approach, conform to the trend of sustainable development [17, 18].

However, using extracts of natural products as the sole reducing agent usually resulted in nanoparticles containing impurities and with low crystallinity [19]. Therefore, combining natural extract and chemical reducing agent have been employed to synthesize magnetite nanoparticles, e.g., combining α-D-glucose and NH_3 solution [20]; green tea extract and NaOH [19]. In the past two decades, there has been an increased focus on green chemistry and cleaner processes. Utilization of natural extracts, environmentally benign solvents and renewable materials are some of the main emphases in a green process. In Vietnam, Citrus aurantifolia fruit is popular and inexpensive. Using Citrus aurantifolia fruit extract as a reducing agent is more environmental friendly and suitable for sustainable development. These green methods to synthesize MNs are expected to replace or reduce the utilization of sodium borohydride which was a commonly used reducing agent in MNs synthesis.

In this work, mixture of Citrus aurantifolia fruit extract and $NaBH_4$ was used in producing MNs using to remove Cr(VI) in aqueous solution. The parameters of synthesis reaction investigated include the volume ration of Citrus aurantifolia extract to $NaBH_4$, reaction time and temperature. For the adsorption of Cr(VI), the effects of pH, reaction time, adsorbent dose and concentration of Cr(VI) on removal efficiency were studied.

Experimental

Materials

The following reagents and chemicals were needed in ferromagnetic synthesis and adsorption experiments: potassium dichromate ($K_2Cr_2O_7$), 1,5-diphenylcarbazide (DPC), sulfuric acid (H_2SO_4), ferrous chloride tetrahydrate ($FeCl_2.4H_2O$, 98%), sodium borohydride ($NaBH_4$, 98%), polyethylene glycol (PEG), Poly(vinylpyrrolidinone) (PVP), hexadecyltrimethylammonium bromide (CTAB, 98%), and ethanol (96%). They were purchased from Sigma Aldrich and directly used without further purification. Limes were collected from the local markets in Can Tho city, Vietnam. Freshly prepared double distilled water was used throughout the experiments.

Green synthesis of iron nanoparticles

A flow chart depicting Fe_3O_4 synthesis by using *Citrus aurantifolia* (lime) extract and $NaBH_4$ is given Fig 1. The solution of lime extracts was firstly prepared. Limes were bought in the local market in Can Tho city and carefully washed with clean water. After squeezing the limes, the collected juice was vacuum filtered using Whatman No.1, 90 nm filter paper. Centrifugation was applied to remove suspended non-solubles. The extracts of lime were used immediately after centrifugation to minimize oxidation. Moreover, pH of each lime extract was determined and properly adjusted to keep it constant.

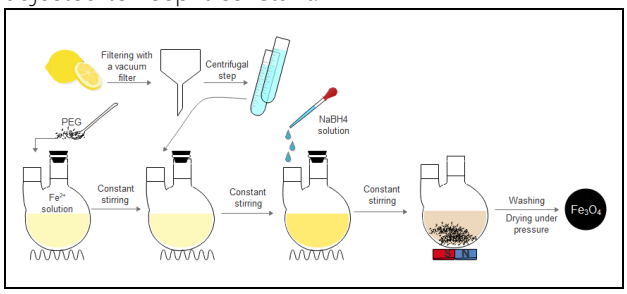

Figure 1: Flow chart of Fe_3O_4 synthesis using *Citrus aurantifolia* fruit extract and sodium borohydride

In the synthesis of MNs, the precursor and the reducing agent were mixed in a beaker. A desired amount of $FeCl_2.4H_2O$ solution (0.2 M) and PEG surfactant solution (1% of the total volume of reactive solution) were added and stirred at room temperature for 60 min. Then 10 mL of the prepared lime extract

was added to the above mixture and stirred continuously for 15 min. When the color of the solution changed from light green to lemon yellow, 20 mL of 0.3 M aqueous $NaBH_4$ solution was added dropwise into the solution. The color of the solution in changed to black, indicating the formation of Fe_3O_4. The precipitate of Fe_3O_4 nanoparticles were collected by applying an external magnet, and the nanoparticles were washed with water and ethanol 96% until the neutral pH. The nanoparticles were dried at 60 °C until the mass was constant. Each reaction was repeated at least two times.

Characterization of magnetic nanoparticles

Fe_3O_4 nanoparticles obtained were characterized. X-ray diffraction (XRD) was performed on a D8 Advance instrument (Bruker), with an X-ray diffractometer using CuK radiation (λ=1.54056 Å) scanned at 7.0000 degree/min, accelerating voltage of 40 kV and applied current of 30 mA. Fourier transform infrared (FTIR) spectra were obtained using a NICOLET 6700 (Thermo) spectrophotometer (frequency range from 4000 to 500 cm^{-1}) with KBr pellet. Field emission scanning electron microscopy (FE-SEM) measurements and energy dispersive X-ray spectroscopy module ADAX (EDX) were taken with a Hitachi S-4800 scanning electron microscopy at accelerating voltage of 10 kV, working distance of 1.8 mm, low magnification mode. Transmission electron microscopy (TEM) were taken on a JEOL-1010 (Japan Electron Co.) and operated at operating valtage of 80 kV, magnification of 60.000x to 100.000x. UV-vis absorption spectra were recorded on a V730 Jasco spectrophotometer operated with single monochromator, silicon photodiode detectors, wide wavelength range of 190 to 1100 nm, fixed bandpass 1.0 nm, speed scanning speed at 8,000 nm/min. The magnetic properties of the sample were investigated using a vibrating sample magnetometer (VSM) on Microsence EZ9, USA operated with maxiumum field of 22.5 kOe, field resolution of 0.001 Oe, signal noise of 0.1 μemu and at room temperature.

Adsorption experiments

A stock of Cr(VI) solution (1000 mg/L) was firstly prepared by dissolving $K_2Cr_2O_7$ in deionized water. All working solutions at the desired concentration were prepared from this stock solution by diluting with deionized water. The initial pH was adjusted to between 2.0 and 6.0 with 0.1 M HCl or 0.1 M NaOH solution. The concentration of Cr(VI) and adsorbent dose were varied from 20 – 150 mg/L and 0.01 – 0.2 mg, respectively. Contact time of adsorbent and the solution studied was from 15 to 75 min. Concentrations of Cr(VI) were determined by using a UV-Vis spectrophotometer at λ= 540 nm after reacting with DPC. The removal capacity of MNs (H%) and the equilibrium adsorption amount (q_e, mg/g) were calculated using the following equations [21].

$$H(\%) = \frac{(C_0 - C_e)}{C_0} \times 100 \quad (1)$$

$$q_e = \frac{(C_0 - C_e) \times V}{m} \quad (2)$$

where C_0 (mg/L) and C_e (mg/L) are the initial concentration and the equilibrium concentration of Cr(VI) solution, respectively. V (L) is the volume of the solution and m (g) is the adsorbent dose.

Results and discussion

Synthesis mechanism

Superparamagnetic Fe_3O_4 nanoparticles could be obtained by the Fe^{2+} controlled particle reduction using Citrus aurantifolia fruit extract which is rich in citric acid. A possible formation mechanism of magnetite nanoparticles by this green method is described in Fig 2. In the reaction system containing $FeCl_2$ and the Citrus aurantifolia extract, the C=O of carboxylic group in citric acid chelated with Fe^{2+} to form complex $COO^-...Fe^{2+}$, while Fe^{2+} was also partially oxidized by H^+ from citric acid to form $COO^-...Fe^{3+}$ complex. Besides, $NaBH_4$ was dispersed in the aqueous solution (Reaction 1), which was the main source to produce OH^- [22].

$$NaBH_4 + H_2O \rightarrow BH_3 + NaOH + H_2 \quad \text{(Reaction 1)}$$

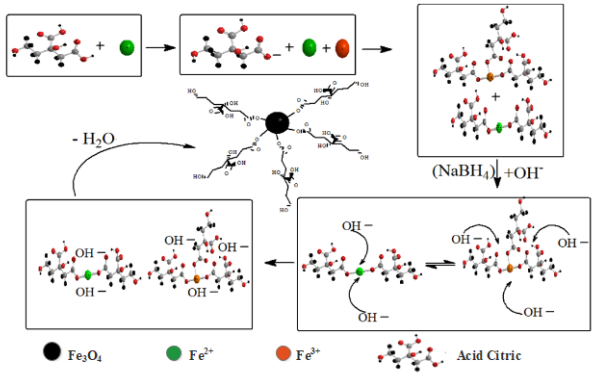

Figure 2: A schematic illustration of the formation mechanism of magnetite nanoparticles

https://doi.org/10.51316/jca.2021.074

Interaction between $COO^-...Fe^{2+}$ bonding and $COO^-...Fe^{3+}$ bonding by OH^- in solution formed $OH^-...Fe^{2+}$ bonding and $OH^-...Fe^{3+}$ bonding, resulting in the formation of both ferric hydroxide, $Fe(OH)_3$ and ferrous hydroxide, $Fe(OH)_2$. Magnetite nanoparticle crystals were formed by dehydrating between ferric hydroxide and ferrous hydroxide [23]. The change of solution color from light green to greenness-yellow, as Citrus aurantifolia extract was added, possibly caused the appearance of the complex of both Fe^{2+} and Fe^{3+}. The Fe_3O_4 magnetite nanoparticles could be drawn from the solution to the wall of the vial by applying an external magnetic field (Fig 3). MNs were obtained after washing with water and ethanol (96%), then dried in atmospheric pressure. These processes were summarized in Reaction 2:

$$Fe^{2+} + Fe^{3+} + 8OH^- \rightarrow Fe_3O_4 + 4H_2O \quad \text{(Reaction 2)}$$

Figure 3: Digital photograph of the Fe_3O_4 nanoparticles synthesized in the presence of a magnet

Evaluation of synthesized MNs properties

X-ray Diffraction (XRD)

MNs prepared from different Citrus aurantifolia extract volume of 2, 5, 8, 10 and 15 mL are referred to as MNs-2, MNs-5, MNs- 8, MNs-10 and MNs-15, respectively (Fig 4a). MNs-60m, MNs-90m and MNs-120m represents reaction time of 60 min, 90 min and 120 min, respectively (Fig 4b), while MNs-30t, MNs-55t and MNs-80t represents reaction temperature of 30 °C, 55 °C and 80 °C, respectively (Fig 4c). The effects of surfactants such as PEG, CTAB, PVP on MNs formation were also investigated.

In Fig 4, the peaks at 2θ = 30.1°, 35.4°, 43.1°, 53.4°, 56.9° and 62.5° refer to (220), (311), (400), (422), (511) and (440) lactic planes, respectively. This observation matched well with the inverse spinel structure of Fe_3O_4 (JCPDS card no. 75–1610) according to the reflection peak positions and relative intensities, which confirmed that the nanoparticles synthesized in this study were the Fe_3O_4 nanoparticles. This indicates that Fe_3O_4 magnetite nanoparticles can be synthesized by green method. Meanwhile, the Bragg reflection peaks were all relatively broad because of the extremely small dimensions of the Fe_3O_4 nanoparticles. The average size of the products could be obtained from Scherrer's equation (3). The calculated size was 43.3 nm.

$$d = \frac{k.\lambda}{\beta.\cos(\theta)} \quad (3)$$

where d is particle diameter, λ is X-ray wave length, β is the peak width of half-maximum, and θ is diffraction angle – Bragg angle, k is the Scherrer constant with the value from 0.9 to 1.

The XRD patterns of MNs synthesized using different extract volumes show stronger and clearer intensity as more Citrus aurantifolia extract was added, and the XRD patterns of MNs-10 and MNs-15 are very similar (Fig 4a). Base on the mechanism, the more H^+ ions from citric acid were dissociated, the more Fe^{3+}complexes oxidized from Fe^{2+} complexes were formed. These complexes were, then, dehydrated to form Fe_3O_4 nanoparticles (Reaction 2). In Fig 4a, MNs-10 showed the highest crystallinity among all MNs. Hence, 10 mL extract was chosen for further experiments.

Figure 4b reveals that the capacity of CTAB and PVP affecting the crystallization of MNs. In aqueous solution, CTAB is a cationic surfactant and forms micelles. Lipophilic biomolecules like polyphenol and flavonoid (which are the major components in Citrus aurantifolia extract) tend to be incorporated into the micellar phase. This progress will prevent the formation of crystalline MNs. PVP is a non-ionic surfactant which can be dissolved in a wide range of organic solvents and water. Characterization of the oxidized nano-fluids revealed the formation of amorphous ferromagnetic ferric oxide phase in the presence of PVP. Thus, PVP is unable to protect the surface oxidation of MNs. In this work, PEG showed better protection MNs oxidation than PVP and CTAB. Besides, PEG is more environmental friendly so PEG is the best option for MNs synthesis.

In Figure 4c and Fig 4d, the appearance of nanoscale zero-valent iron (nZVI) is obvious due to the observed characteristic peaks at 2θ = 44.9° corresponding to

nZIV (α-Fe) [24, 25]. Actually, Figure 4c shows phase transition of Fe_3O_4 to nZVI as reaction temperature was elevated from ambient temperature to higher temperature (55 °C and 80 °C). At 55 °C, a mixture of MNs and nZVI was observed, but the only nZVI was found at 80 °C. Thus, ambient temperature was selected in studying the effect of reaction time. In other studies which synthesized MNs mostly were conducted under high temperatures [26, 27], yet this study indicated that MNs can be synthesized at room temperature. As can be seen in Fig 4d, as reaction time was extended to 90 min and 120 min, nZVI was again appeared. The presence of nZVI can be attributed to aromatic groups derived from lime extract as shown in Reaction 3 [28], where Ar stands for aromatic group.

$$nFe^{2+} + 2Ar\text{-}(OH)_n \rightarrow nFe^0 + 2nAr\text{-}O + 2nH^+ \quad \text{(Reaction 3)}$$

As temperature increases, the reaction rate of Reaction 3 increases, resulting in concomitant reduction reaction of Fe_3O_4 nanoparticles to nZVI. The presence of aromatic groups in lime extract was confirmed by FTIR analysis (Figure 5) and EDS analysis (Figure 7).

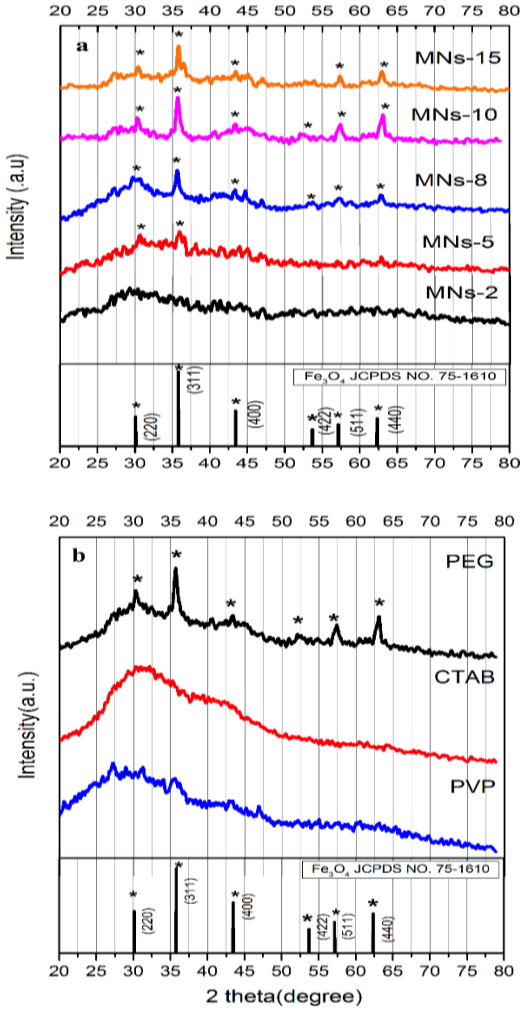

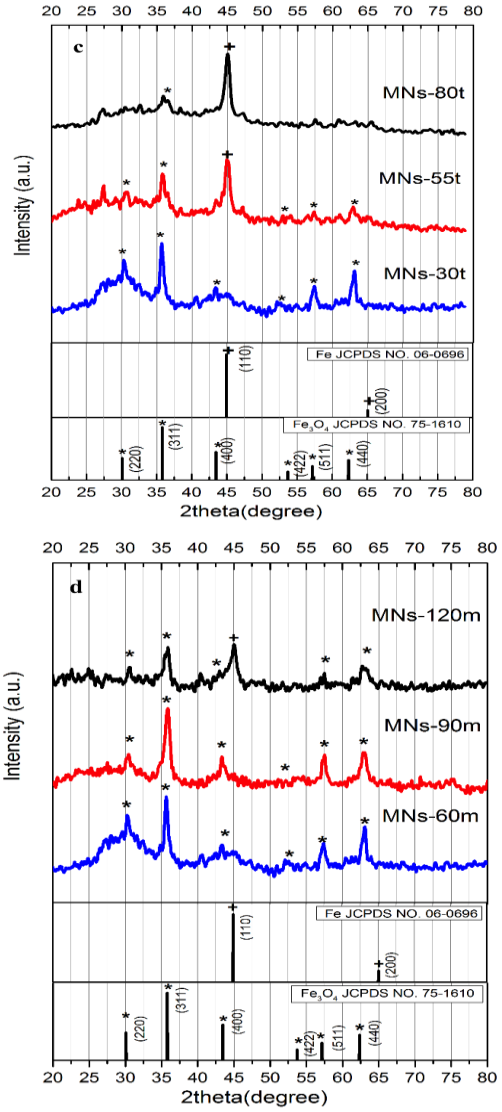

Figure 4: XRD of synthesized magnetite nanoparticles. Different volumes of lime extract (2 mL, 5 mL, 8 mL, 10 mL and 15 mL); (b) Different surfactants (PEG, CTAB, and PVP) (c) Different reaction temperatures (30 °C, 55 °C and 80 °C); (d) Different reaction times (60 min, 90 min, and 120 min)

Fourier Transform Infrared Spectroscopy (FT-IR)

The FTIR spectrum (Fig 5) reveals a broadband at 3381.8 cm^{-1}, corresponding to traces of water on MNs surface, which was assigned to O–H stretching vibrations. The absorption peaks at 1622.5 and 1422.8 cm^{-1}, respectively indicate the C=C and C–C aromatic ring stretching vibration of polyphenolic compounds which are abundant in many plant extracts [17, 29, 30]. The absorption peak at 1384.1 cm^{-1} can be assigned to O–H bending vibration. The aromatic ring showed a characteristic signal at 873.6 cm^{-1}. The intensive absorption band at 575.3 cm^{-1} was assigned to Fe–O

bonding in Fe_3O_4 nanoparticles [7, 28, 31]. Table 1 is a summary of the FTIR peaks and the corresponding mode assignments Therefore, MNs formed by using Citrus aurantifolia extract was confirmed by FITR analysis and this MNs adsorbed polyphenolic compounds onto its surface.

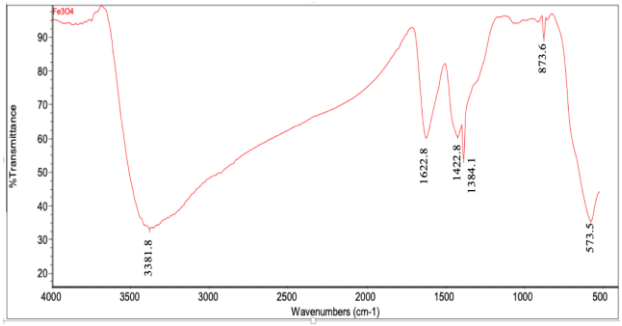

Figure 5: FTIR profile of green synthesized nanoparticles

Table 1: FTIR peaks and corresponding mode assignments for MNs from lime extract

No	Wavenumber (cm^{-1})	Peak assignment
1	3381.8	O–H stretching
2	1622.5	C=C stretching (aromatic)
3	1422.8	C–C stretching (aromatic)
4	1384.1	O–H bending
5	873.6	Aromatic ring
6	575.3	Fe–O bonding

Transmission Electron Microscopy (TEM) and Field Emission Scanning Electron Microscope (FE-SEM)

Surface morphology of MNs synthesized using 10 mL lime extract and 40 mL 0.3 M $NaBH_4$ solution was analyzed by FE-SEM. The FE-SEM image (Fig 6a) shows that as-synthesized MNs were roughly spherical with narrow size distribution. These spherical shapes were formed due to isotropic nucleation rate per unit area at the interface between MNs [32] which was the driving force for Ostwald ripening. The surface free energy was minimum by reduction of total surface area per volume, resulting in equivalent growth rate along with nucleation in different directions because sphere has the smallest surface area per unit volume of any shape [20]. Additionally, surface energy increased by the great number of charges distributed on the MNs surface, so the spherical shape indicated that surface tension is higher than larger particles [17]

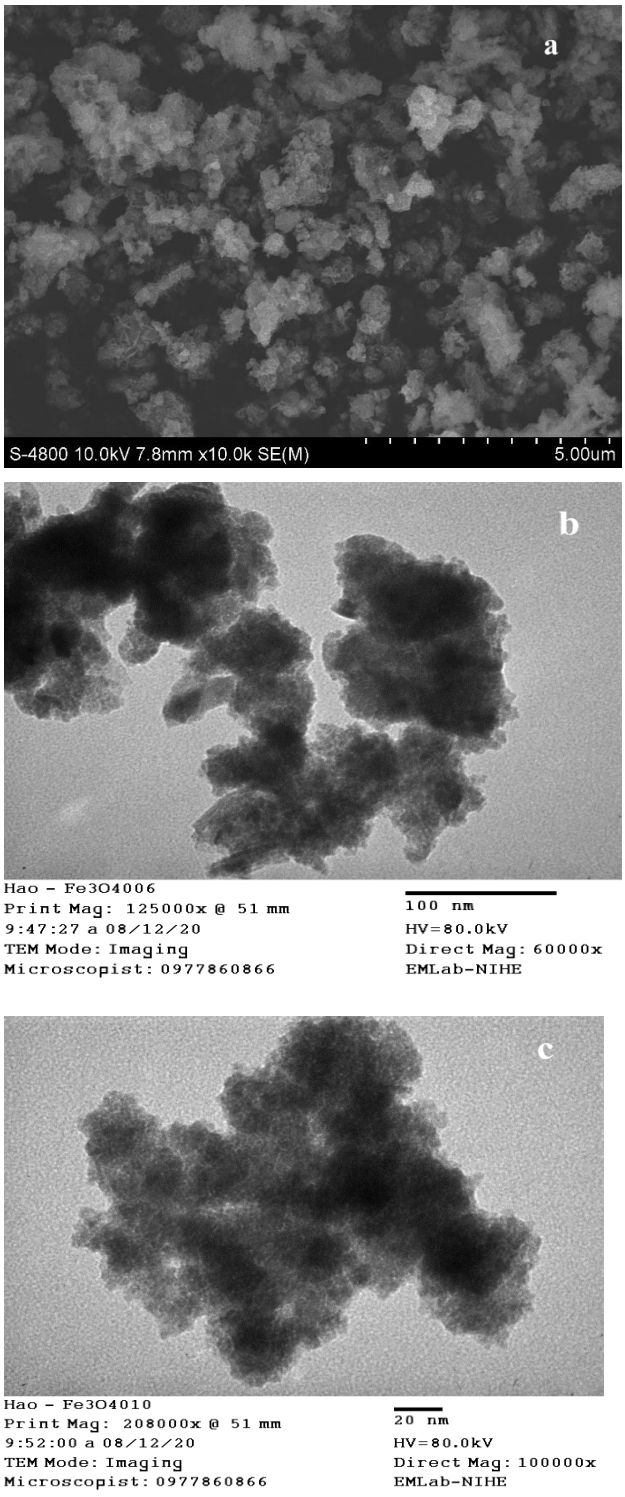

Figure 6: Images of synthesized MNs using lime extract and $NaBH_4$ at optimal condition: 90 min, 30 °C and 10 mL of lime extract; a. FE-SEM, b. TEM (scale 100 nm), c. TEM (scale 20 nm)

The size and shape of MNs were determined by TEM analysis. As shown in Fig 6b and Fig 6c, TEM analysis

reveals that MNs both spherical and elliptical particles were formed. The TEM image shows that the sizes of the MNs were approximately between 40 and 60 nm. The good correlation of particle sizes obtained from the Scherrer's equation in XRD pattern and TEM supports the crystalline structure of Fe_3O_4 nanoparticles.

Energy Dispersive X – ray Fluorescence Spectrometry (EDX)

The EDX spectrum of the powder MNs sample (Fig 7) shows the presence of Fe, O, and C elements with 53%, O 41.74%, and 4.96% composition, respectively (Table 2). The strong peaks of Fe observed at around 0.8, 6.2 and 6.9 keV, and the intensive peak of O at 0.6 keV were related to the binding energies of O. Therefore, these peaks correspond to the presence of Fe_3O_4. However, the impurity peak of C was found at 0.4 keV due to the presence of bio-organic components in Citrus aurantifolia extract, which were adsorbed on the surface of Fe_3O_4 nanoparticles. This finding was also observed by FITR spectra in Fig 5. FTIR peaks at 1622.5, 1422.8 and 873.6 show the appearance of aromatic rings. Due to significant amount of acid citric presented in the reaction, acid ascorbic likely remained in solution. Table 3 shows compounds predicted in MNs base on atomic ratios.

Table 2: Percentages of weight and atomic by EDX spectra

Element	%Weight	%Atomic
C K	4.96	10.38
O K	41.74	65.62
Fe K	53.30	24.00
Total	100.00	

Table 3: Compounds predicted in MNs base on atomic ratio

Compounds	%Fe	%O	%C
Fe_3O_4	24.00	32.00	-
$C_6H_8O_6$ (Ascorbic acid)	-	10.38	10.38
H_2O	-	23.24	-
Total	24.00	65.62	10.38

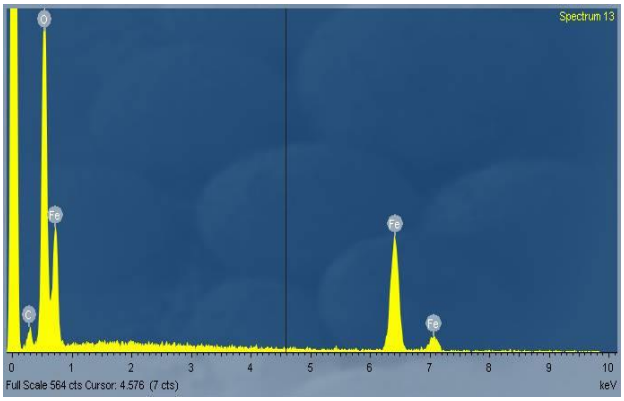

Figure 7: EDX spectra of Fe_3O_4 synthesized at optimal reaction conditions

Vibrating Sample Magnetometer (VSM)

The magnetization curve measured for the as-synthesized Fe_3O_4 nanoparticles in this study is presented in Fig 8. The measured specific saturation magnetization value of MNs was 40.1 emu/g. The low specific saturation magnetization in MNs with particle size of several tens of nanometers was feasibly due to the presence of non-magnetic layer on the particle surface, cation distribution and superparamagnetic relaxation. However, the negligible coercivity Hc of hysteresis loop (195.7 Oe) and consequently low remanence Ms (5 emu/g) indicate the superparamagnetic nature of the MNs.

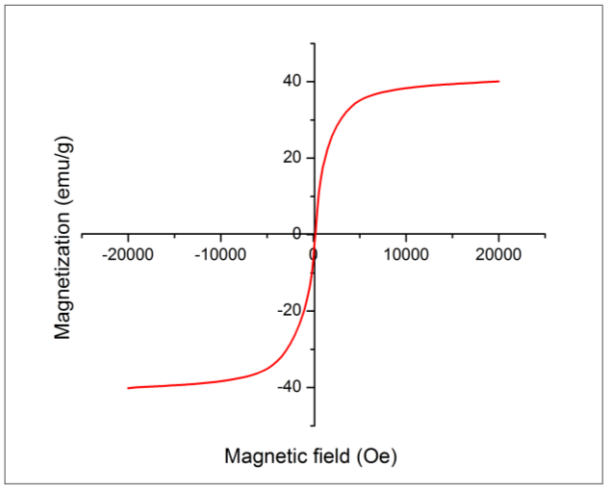

Figure 8: Magnetization curve of Fe_3O_4 synthesized using lime extract and $NaBH_4$

In this work, experiments were carried out at room temperature (30 °C) compared to those reported under higher temperatures (Table 4). MNs in this study can be produced easily at room temperature. The synthesized nanoparticle sizes were bigger than those of other studies but with more uniform size achieved

https://doi.org/10.51316/jca.2021.074

by using surfactants. In conclusion, the process was evaluated as a simple method for MNs synthesis.

Hexavalent Chromium adsorption

Effect of pH on Cr(VI) removal

The adsorption ability of MNs toward Cr(VI) in a pH range of 2.0 to 8.0 and the results are presented in Figure. 9 and Table 5. As can be seen, pH of the solution significantly influenced the adsorption capacity. Both adsorption yield (~94.8%) and capacity (47.4 mg/g) were almost constant in the pH range of 2.0 to 3.0. The yield decreased to about 88% as pH was increased to 4.0 ~ 5.0. After that the yield dropped sharply as pH continued to increase, reaching 71.2% at pH 8. Similar trend was also observed for adsorption capacity.

Table 4: The comparison of the obtained results between this work and the published works

Reactants (Fe^{2+}/Fe^{3+})	Reaction conditions				Size of MNs (nm)	References
	Reducing agent	Using of plant extract	Temperature (°C)	Time (min)		
Fe^{2+}/Fe^{3+}	NaOH	Ipomoea aquatica leaf extract	N.R.	N.R.	18	[10]
Fe^{2+}/Fe^{3+}	NH_4OH and α-D-glucose	N.R.	60	30	0.25	[13]
Fe^{2+}	NaOH	Camellia angustifolia leaves	60	120	5-10	[30]
Fe^{2+}	$NaBH_4$	Citrus aurantifolia extract	Room temperature	90*	40	This work

*90 min include 60 min for homogenously stirring and 30 min for time reaction between Citrus aurantifolia extract and Fe^{2+}, N.R.: not reported

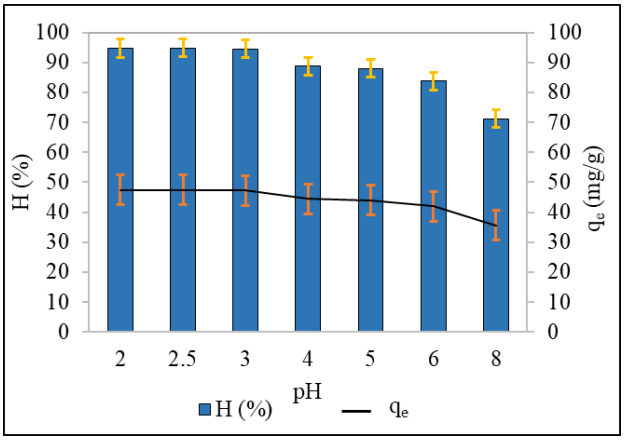

Figure 9: Effect of pH on Cr(VI) removal (Initial concentration: 100 mg/L, reaction temperature: 25 °C, adsorbent dose: 0.15 g, reaction time: 45 min)

From the above observation, MNs showed strong adsorption at pH less than 3.0. The main reason could be that Cr(VI) mainly existed in the form of $Cr_2O_7^{2-}$ and $HCrO_4^-$ in a pH range of 2.0 to 6.0, and then the CrO_4^{2-} species became dominant at higher pH [33]. In the meantime, Figure 10 shows that the surface of MNs is strongly protonated in a solution containing more protons. The positive surface charge of MNs was high in pH range of 2.0 to 3.0 and then slightly reduced as pH rose. The significant reduction of positive surface charge of MNs occurred as pH was higher than 6.0. In other words, the adsorption capacity of MNs toward negatively charged species could be significantly decreased as pH of the solution increased higher than 6.0 due to a weak electrostatic interaction [21].

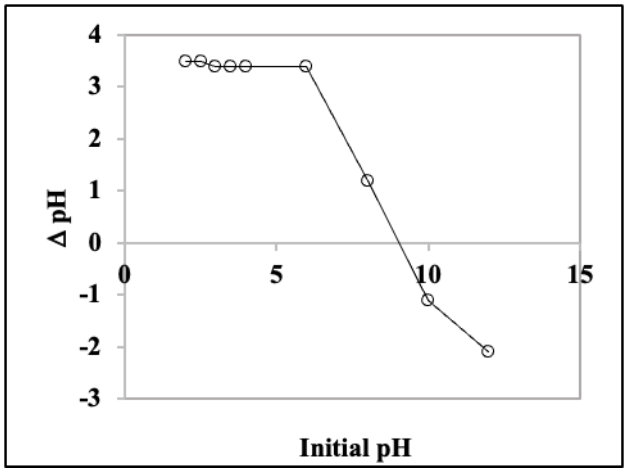

Figure 10: Surface charge of Fe_3O_4 nanoparticles as a function of initial pH

Based on the above explanation, the main mechanism of the adsorption in this work was electrostatic interaction. In conclusion, the adsorption ability of MNs is highly depended on pH of the solution. The highest adsorption yield (94.6%) and capacity (47.5 mg/g) of MNs was obtained at pH 2.5. Therefore, all the further experiments were conducted at pH 2.5.

Effect of contact time on Cr(VI) removal

Contact time (reaction time) has significant effect on adsorption. In this work, reaction time varied from 15 to 75 min and the adsorption results are presented in Fig 11 and Table 6. The Cr(IV) removal raised from 83.7% to 94.7% as reaction time increased from 15 min to 45 min, the change in Cr(VI) removal was insignificant after 45 min. Similar trend was observed for the equilibrium adsorption amount qe. Apparently 45 min was enough for Cr(VI) to diffuse from bulk solution to the surface of Fe_3O_4 nanoparticles and be adsorbed [34].

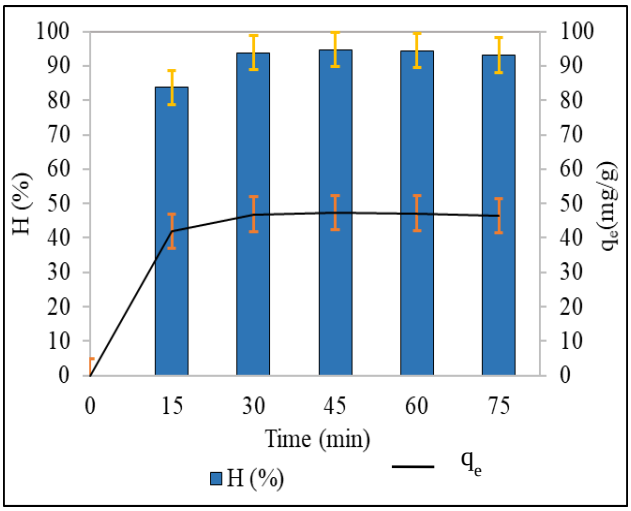

Figure 11: Effect of reaction time on Cr(VI) removal (Initial concentration: 100 mg/L, pH 2.5, reaction temperature: 25 °C, adsorbent dose: 0.15 g)

Effect of Fe_3O_4 nanoparticles dose on Cr(VI) removal

As seen from Figure 12, adsorbent dose strongly affect the removal yield of Cr(VI). As the adsorbent dose was increased from 0.01 to 0.1 g, the removal percentage of Cr(IV) increased from 16.8% to 94.8% (a 5.64-fold increase). Removal capacity remained constant after that. On the other hand, as dose was increased from 0.01 to 0.2 g, equilibrium adsorption amount decreased from 84.0 to 23.8 mg/g. This result shows at low dose the active adsorption sites were not enough, so multilayer adsorption occurred. On the other hand, single layer adsorption was the predominant adsorption mechanism at high adsorbent dose. A dose of 0.1 g were applied for further experiments.

Effect of Cr(VI) concentration

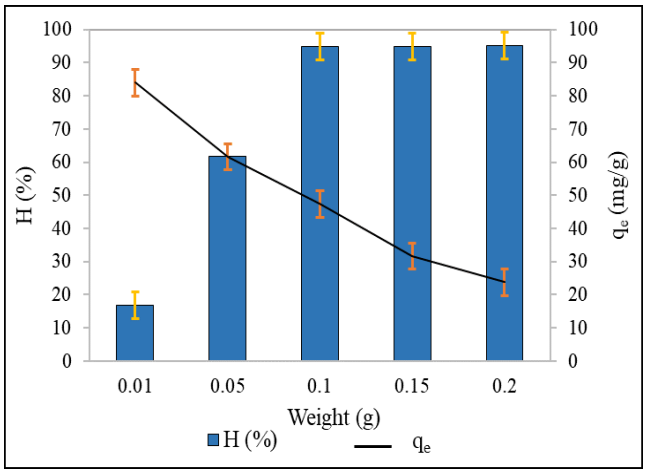

Figure 12: Effect of Fe_3O_4 nanoparticles dose on Cr(VI) removal (Initial concentration: 100 mg/L, pH 2.5, reaction temperature: 25 °C, reaction time: 45 min)

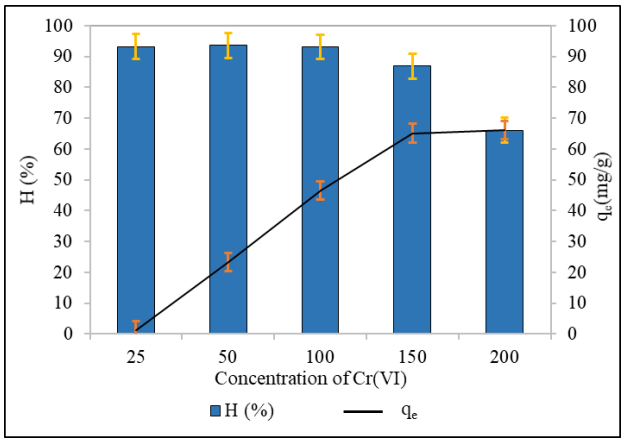

Figure 13: Effect of Cr(VI) concentration on the removal (pH 2.5, reaction temperature: 25 °C, reaction time: 45 min, adsorbent dose: 0.1g)

Figure 13 shows that removal capacity of Cr(IV) was constant (~ 93%) as Cr(VI) concentration was increased from 25 to 100 mg/L, it then decreased to 47.1% as Cr(VI) concentration was increased to 200 mg/L. For equilibrium adsorption amount (q_e), it increased from 11.7 mg/g at a Cr(VI) concentration of 25 mg/L to 65.2 mg/g at a Cr(VI) concentration of 150 mg/L, then slightly increased to 66.1 mg/g as Cr(VI) concentration was at 200 mg/L (Table 8). The results indicate that at low Cr(VI) concentration (<100 mg/L), there were enough active sites for Cr(VI) adsorption, hence almost constant adsorption yield was observed. However, at Cr(VI) concentration >100 mg/L, the active sites of MNs

https://doi.org/10.51316/jca.2021.074

were not enough to adsorb more Cr(VI) due to saturation. Consequently, the optimum concentration for Cr(VI) adsorption is 150 mg/L.

Adsorption isotherms

To gain insight of adsorption mechanism of Cr(VI) onto MNs, data were fitted with Langmuir, Freundlich, and Dubinin-Radushkevich models. As shown in Table 9, Langmuir isotherm model gave the best fit in term of its highest value of R^2. This result suggests that the monolayer adsorption of Cr(VI) occurred. The maximum adsorption capacity of Cr(VI) onto MNs from the fitted Langmuir model is 72.46 mg/g (Table 9). In Table 9, in the Freundlich model a n value of 2.18 confirms the removal Cr(VI) ability of MNs is a good fit. Besides, the dimensionless parameter (RL) also evaluates the favorability of adsorption of Cr(VI) onto MNs following the Langmuir isotherm model. The value of RL for Cr(VI) adsorption onto MNs were between 0 and 1, indicating that the process is favorable. More detail can be obtained from the Dubinin-Radushkevich isotherm model. The free energy in Cr(VI) adsorption by MNs surface was 0.87 kJ/mol. A value of E under 8 kJ/mol indicates physical adsorption [35-36].

Table 9: Fitted isotherm models for Cr(VI) adsorption onto Fe_3O_4

Isotherms	Unit	Information
Freundlich model: Fitted model		$\log q_e = 1.164 + 0.4568 \ln C_e$
K_F	-	13.07
n	$(mg/g)^{1/n}$	2.18
R^2	-	0.806
Langmuir model: Fitted model		$C_e/q_e = 0.0786 + 0.0138C_e$
KL	L/mg	0.176
Q_{max}	mg/g	72.46
R^2	-	0.9911
$RL = 1/1+K_LC_i$		From 0.05 to 0.76
D-R: Fitted model		$\ln q_e = 2.6043 - 0.6557\varepsilon^2$
E	kJ/mol	0.87
K_{DR}	mol^2/kJ^2	0.6557
R^2	-	0.6822

Conclusions

Magnetite nanoparticles (Fe_3O_4) were synthesized by *Citrus aurantifolia* extract combined with $NaBH_4$ in this study. Although the phenolic and acid citric level in *Citrus aurantifolia* extract were not stable, the combination of plant extract and $NaBH_4$ was able to synthesize MNs. The green method in the present work has advantageous in the synthesis of magnetite nanoparticles such as it is economical, environmentally friendly, non-toxic. The spherical and elliptical magnetite nanoparticles in size of 40-60 nm can be obtained in one-pot reaction at mild conditions, namely 10 mL extract combined with 20 mL $NaBH_4$ 0.3 M with the present of PEG at room temperature for 60 min. The as-synthesis magnetite nanoparticles (Fe_3O_4) were capable of removal Cr(VI) in solution with a q_{max} of 71.94 mg/g, suggesting potential application in environmental treatment.

Acknowledgments

This research is funded by Vietnam National Foundation for Science and Technology Development (NAFOSTED) under grant number 103.02-2020.64.

References

1. Z. Rahman, V.P. Singh, Environ. Monit. Assess. 191 (2019) 419-439. https://doi.org/10.1007/s10661-019-7528-7
2. S. Mahdavi, S.R. Allahkaram, J. Alloy. Compd. 635 (2015) 150-157. https://doi.org/10.1016/j.jallcom.2015.02.119
3. X.F. Lei, X.X. Xue, H. Yang, C. Chen, X. Li, J.X. Pei, M.C. Niu, Y.T. Yang, X.Y. Gao, J. Alloy. Compd. 646 (2015) 541-549. https://doi.org/10.1016/j.jallcom.2015.04.233
4. P. Yuan, D. Liu, M. Fan, D. Yang, R. Zhu, F. Ge, J. Zhu, H. He, J. Hazard. Mater. 173 (2010) 614-621. https://doi.org/10.1016/j.jhazmat.2009.08.129
5. S. Aredes, B. Klein, M. Pawlik, J. Clean. Prod., 60 (2013) 71-76. https://doi.org/10.1016/j.jclepro.2012.10.035
6. J. Saini, V.K. Garg, R.K. Gupta, J. Mol. Liq. 250 (2018) 413-422. https://doi.org/10.1016/j.molliq.2017.11.180
7. S.N. Wang, F.D. Zhang, A.M. Huang, Q. Zhou, De Gruyter 70 (2016) 503-510. https://doi.org/10.1515/hf-2015-0125

8. Z. Wang, J. Xu, Y. Hu, H. Zhao, J. Zhou, Y. Liu, Z. Lou, X. Xu, J. Taiwan Inst. Chem. E. 60 (2016) 394-402. https://doi.org/10.1016/j.jtice.2015.10.041
9. H. Zhang, G. Zhu, Appl. Surf. Sci. 258 (2012) 4952-4959. https://doi.org/10.1016/j.apsusc.2012.01.127
10. J. Wang, S. Zheng, Y. Shao, J. Liu, Z. Xu , D. Zhu, J. Colloid. Interf. Sic. 349 (2010) 293-299. https://doi.org/10.1016/j.jcis.2010.05.010
11. C.M. Babu, Babu, B. Palasinamy, B. Sundaravel, M. Palachinamy, V. Murugesa, J. Nanosci. Nanotechno. 13 (2013) 2517-2527. https://doi.org/10.1166/jnn.2013.7376
12. S.H. Chaki, T.J. Malek, M.D. Chaudhary, J.P. Tailor, M.P. Deshpande, Adv. Nat. Sci: Nanosci. Nanotechnol. 6 (2015) 035009-035014. http://dx.doi.org/10.1088/2043-6262/6/3/035009
13. A. Ruíz-Baltazar, R. Esparza, G. Rosas, R. Pérez, J. Nanomater. 2015 (2015) 1-8. https://doi.org/10.1155/2015/240948
14. S.A. Jayanthi, D.M.G.T. Nathan, J. Jayashainy, P. Sagayaraj, Mater. Chem. Phys. 162 (2015) 316-325. https://doi.org/10.1016/j.matchemphys.2015.05.073
15. C. Meng, W. Zhikun, L. Qiang, L. Chunling, S. Shuangqing, H. Songqing, J. Hazard. Mater. 341 (2018) 198-206. https://doi.org/10.1016/j.jhazmat.2017.07.062
16. T.T. Tung, J. Feller, T. Kim, H. Kim, W.S. Yang, K.S. Suh, J. Polym. Sic. A1. 50 (2012) 927-935. https://doi.org/10.1002/pola.25847
17. M.M. Zaman, D.M.A.S Karal, D.M.N.I. Khan, A.R.M. Tareq, S. Ahammed, D.M. Akter, A. Hossain, A.K.M.A. Ullah, ChemistrySelect. 4 (2019) 7824-7831. https://doi.org/10.1002/slct.201901594
18. S. Ahmadian-Fard-Fini, M. Salavati-Niasari, D. Ghanbari, SAA. 2203 (2018) 481-493. https://doi.org/10.1016/j.saa.2018.06.021
19. T. Shahwan, S.A. Siriiah, M. Nairat, E. Boyaci, A.E. Eroğlu, T.B. Scott, K.R. Hallam, Chem. Eng. J. 172 (2011) 258-266. https://doi.org/10.1016/j.cej.2011.05.103
20. W. Lu, Y. Shen, A. Xie, W. Zhang, J. Magn. Magn. Mater. 322 (2010) 1828-1833. https://doi.org/10.1016/j.jmmm.2009.12.035
21. S. Li, L. Liu, Y. Yu, G. Wang, H. Zhang, A. Chen, J. Alloy. Compd. 698 (2017) 20-26. https://doi.org/10.1016/j.jallcom.2016.12.163
22. S. Chandrasekhar, A. Shrinidhi, Synthetic Commun., 44 (2014) 2051-2056. https://doi.org/10.1080/00397911.2014.888751
23. A.M. Awwad, N.M. Salem, Nanosci. Nanotechnol. 2 (2012) 208-213. https://doi: 10.5923/j.nn.20120206.09
24. T. Wang, J. Su, X. Jin, Z. Chen, M. Megharaj, R. Naidu, J. Hazard. Mater. 262 (2013) 819-825. https://doi.org/10.1016/j.jhazmat.2013.09.028
25. Y. Kuang, Q. Wang, Z. Chen, M. Megharaj, R. Naidu, J. Coll. Interf. Sci. 410 (2013) 67-73. https://doi.org/10.1016/j.jcis.2013.08.020
26. M. Krajewski, K. Brzozka, W.S. Lin, H.M. Lin, M. Tokarczyk, J. Borysiuk, G. Kowalskia, D. Wasik, Phys. Chem. Chem. Phys. 18(2016) 3900-3909. https://doi.org/10.1039/C5CP07569F
27. L.Y. Zhang, T. Chu, Bulletin of the Korean Chemical Society, 34 (2013) 1457-1461. https://doi.org/10.5012/bkcs.2013.34.5.1457
28. T. Wang, J. Lin, Z. Chen, M. Megharaj, R. Naidu, J. Clean. Prod., 83 (2014) 413-419. https://doi.org/10.1016/j.jclepro.2014.07.006
29. M. Mahdavi, F. Namvar, M.B. Ahmad, R. Mohamad, Molecules 18 (2013) 5954-5964. https://doi.org/10.3390/molecules18055954
30. A.S.Y. Ting, J.E. Chin, Water Air Soil Pollut. 231 (2020) 278. https://doi.org/10.1007/s11270-020-04658-z
31. R.K. Das, B.B. Borthakur, U. Bora, Mater. Lett. (2010) 64 1445-1447. https://doi.org/10.1016/j.matlet.2010.03.051
32. D.K. Kim, M. Mikhaylova, Y. Zhang, M. Muhammed, Chem. Mater. 15 (2003) 1617-1627. https://doi.org/10.1021/cm021349j
33. C.V. Gherasim, G. Bourceanu, R.I. Olariu, C. Arsene, J. Hazard. Mater. 197 (2011) 244-253. https://doi.org/10.1016/j.jhazmat.2011.09.082
34. F. Ghorbani, S. Kamari, Environ. Technol. Innov. 14 (2019) 100333. https://doi.org/10.1016/j.eti.2019.100333
35. G. Moussavi, B. Barikbin, Chem. Eng. J. 162 (2010) 893-900. https://doi.org/10.1016/j.cej.2010.06.032
36. Q. Hu, Z. Zhang, J. Mol. Liq. 277 (2019) 646-648. https://doi.org/10.1016/j.molliq.2019.01.005